Ultrafast microscopy captures the dynamics of bound excitons in twisted bilayer van der Waals materials

Hiral Patel[a], Kyle T. Vogt[a], Lujie Huang[b,c], Jiwoong Park[b,c], Matt W. Graham*[a]
[a] Oregon State University, Department of Physics, Corvallis, OR 97331, USA
[b] Kavli Institute at Cornell for Nanoscale Science, Ithaca, NY 14853, USA
[c] Cornell University, Department of Chemistry, Ithaca, NY 14853, USA

ABSTRACT

Stacking and twisting 2D van der Walls (vdW) materials can create unique electronic properties that are not accessible in a single sheet of material. When two sheets of van der Waals material such as graphene are stacked in an off-axis angle, in a twisted bilayer graphene (*t*BLG) configuration, electronic properties are modified from interlayer orbital hybridization effects. For instance, in *t*BLG we can access both massless and massive chiral quasiparticles characteristics of graphene and bilayer graphene, as well as angle tunable optical resonances that are not present in graphene or bilayer graphene. In addition, first principle simulation predicts that upon optical resonant excitation of *t*BLG, bound exciton formation is a possibility due to cancelation of exciton-continuum coupling from anti-symmetric superposition of degenerate resonant transitions. In order to study possible bound exciton formation, we map out the electronic structure of single grain *t*BLG using multi-photon transient absorption microscopy. Surprisingly, upon resonant optical excitations, *t*BLG shows enhanced transient response with longer carrier lifetime compared to AB stacked bilayer graphene. Further, we find that the origin of this unexpected optical response can be best explained by the presence of a lower lying bound exciton state predicted by recent theoretical simulations. This suggests that *t*BLG is a novel 2D hybrid material that enables the creation of strongly-bound excitons along-side highly-conductive continuum states. Recently, the family of 2D vdW materials has grown appreciably. As such, there are countless possibilities for stacking and twisting 2D vDw materials to produce similar interlayer electronic states for next generation optoelectronics.
Keywords: van der Waals materials, twisted bilayer, ultrafast microscopy, excitons

1. INTRODUCTION

The Physics of 2D van der Walls (vdW) materials and heterostructures is being intensely studied and developed. Material properties of vdW materials change drastically as you go from 3D to 2D[1,2]. Stacking and twisting 2D vdW materials create further unique properties that are not accessible in a single material. Graphene is a 2D structure of carbon atoms arranged in a hexagonal lattice with two-carbon atoms per unit cell[1,2]. It is the thinnest yet the strongest material in the world which is electrically and thermally conductive, elastic, and impermeable to gases[3,4,] . Owing to the linear dispersion relation, the charge carriers in single layer graphene show similarity to massless Dirac fermions[5,6]. In bilayer graphene, at very low energies, the charge carriers are known to be massive chiral quasiparticles with parabolic dispersion relation[7]. While intrinsic bilayer graphene does not have a bandgap, the carrier density in bilayer graphene can be changed by either doping or gating, which enables the electronic properties to be tuned[1,8,9].

In vdW materials, the interlayer distance, stacking type, and rotation angles give rise to the unique electronic, optical, and mechanical properties. Fabrication of graphene with chemical vapor deposition (CVD) show that single layer graphene is often produced with significant amounts of bilayer graphene that include *t*BLG[10,11]. In *t*BLG, two graphene layers are rotated by an arbitrary angle with respect to each other. The rotation angle can be determined using dark-filed transmission electron microscopy (DF-TEM)[12]. It has been shown that photoexcited electrons relax faster than e-h separation timescale for both graphene and bilayer graphene making it prohibitive for highly efficient optoelectronics applications[13]. However, we recently discovered that slower relaxation rate may be possible in metallic *t*BLG due to its unique band symmetry[14,34]. This has been shown theoretical modelling of the e-h interactions, and the simulations predict the existence of strongly-bound excitons in an otherwise metallic material *t*BLG[14]. The existence of bound excitons in *t*BLG opens up a new realm of optoelectronic applications. Beyond graphene, this mechanism for interlayer bound exciton formation is very general and may hold exciting promise for other stacked, twisted 2D vdW materials[14].

*graham@physics.oregonstate.edu; phone 1 541 737-4631; fax 1 541 737-1683; http://physics.oregonstate.edu/energetics/index.html

Ultrafast Bandgap Photonics II, edited by Michael K. Rafailov, Proc. of SPIE Vol. 10193, 101930V

2. REVIEW OF THEORY: *INTERLAYER ELECTRONIC STRUCTURE*

2.1 Electronic band structure of graphene in the tight binding approximation

We begin with a brief review of the electronic structure of graphene to establish a common notation for discussing the interlayer electronic structure of twisted bilayer graphene (*t*BLG) in the later sections. The atomic structure of single layer graphene in Figure 1a shows distinct carbon atoms, A and B, in the unit cell. The lattice vectors are: $\mathbf{a_1} = \sqrt{3}a_0\left(\frac{1}{2},\frac{\sqrt{3}}{2}\right), \mathbf{a_2} = \sqrt{3}a_0\left(-\frac{1}{2},\frac{\sqrt{3}}{2}\right)$ where a_0 is the nearest neighbor distance, $a_0 = 1.42$ Å[15]. Out of the four valence electrons, three are used for sp^2 bonds in carbon. The fourth electron is in a $p_z$orbital, and there are two electrons per unit cell in a $p_z$orbital. Therefore, there are two orbitals, one for atom A, and one for atom B for a unit cell (there are two π- bands, one for each electron). The tight-binding model Hamiltonian: $\hat{H} = \sum_{<r,r'>}(-t\, a_1^{\dagger}(\mathbf{r})a_2(\mathbf{r}))$ + Hermitian Conjugate (HC)[16] can be expanded over the graphene unit cell site basis to obtain,

$$\hat{H} = \sum_{<\mathbf{r},\mathbf{r}'>}\left(-\frac{t}{N}\right)\sum_{\mathbf{kk}'}^{BZ} e^{-i\mathbf{k}\cdot\mathbf{r}}(e^{i\mathbf{k}'\cdot\mathbf{r}'} + e^{i\mathbf{k}\cdot\mathbf{r}}e^{i\mathbf{k}\cdot\boldsymbol{a_1}} + +e^{i\mathbf{k}\cdot\mathbf{r}}e^{i\mathbf{k}\cdot\boldsymbol{a_2}})a_{1\mathbf{k}}^{\dagger}a_{2\mathbf{k}'} + HC$$

here t represents the transfer integral corresponding to electronic hopping between atoms and the Fourier-transformed creation and annihilation operators are defined as,

$a_1^{\dagger}(\mathbf{r}) = \frac{1}{\sqrt{N}}\sum_{\mathbf{k}} e^{-i\boldsymbol{k}\cdot\mathbf{r}}\, a_{1\mathbf{k}}^{\dagger}$, $\quad a_2(\mathbf{r}') = \frac{1}{\sqrt{N}}\sum_{\mathbf{k}'} e^{-i\boldsymbol{k}'\cdot\mathbf{r}'}\, a_{2\mathbf{k}'}$,

Alternatively, this can be expressed in a matrix form, with an oveall phase factor of $e^{-i\boldsymbol{k}'\cdot(\mathbf{r}-\mathbf{r}')}$, as

$$\hat{H} = \sum_{\mathbf{k}}(a_{1\mathbf{k}}^{\dagger}\, a_{2\mathbf{k}}^{\dagger})\begin{pmatrix} 0 & -tf(\mathbf{k}) \\ -tf^{*}(\mathbf{k}) & 0 \end{pmatrix}\begin{pmatrix} a_{1\mathbf{k}} \\ a_{2\mathbf{k}} \end{pmatrix}, \text{ where } f(\mathbf{k}) = \left(1 + e^{i\mathbf{k}\cdot\mathbf{a_1}} + e^{i\mathbf{k}\cdot\mathbf{a_2}}\right). \quad (1)$$

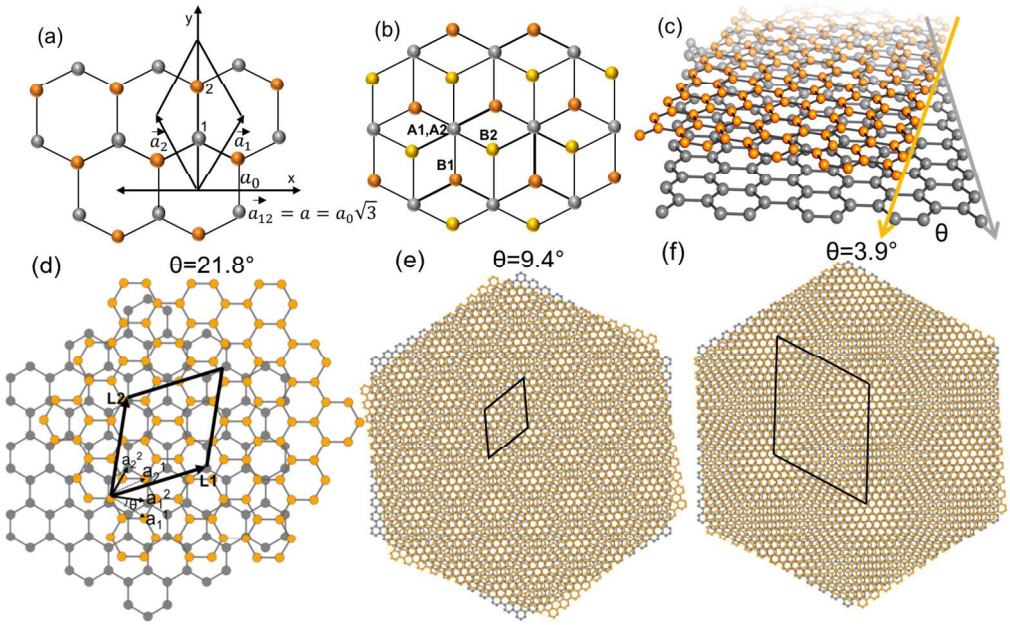

Figure 1. (a) Lattice structure of single layer graphene; Two carbon atoms per unit cell are labeled as 1, and 2 (grey, and orange). Primitive vectors are $\vec{a}_1$, and $\vec{a}_2$, (b) Lattice structure of bilayer graphene. Sub lattices for the lower layer are A1, and B1, and those for the top layer are A2, and B2, with relative positions of atoms projected onto the x-y plane (c) Lattice structure of twisted bilayer graphene for rotation θ, (d) *t*BLG θ=21.8°, with [(m,n)=(1,2)], highlighted unit cell for (e) θ=9.4°, (f) θ=3.9°

The diagonal term H_{AA} corresponds to the orbital interactions between two A atoms, H_{BB} corresponds to the orbital interactions between two B atoms. H_{AB}, and H_{BA} represent hopping between the two sites A, and B. To find the dispersion relation, setting onsite energies, $\varepsilon_A = \varepsilon_B = 0$, and diagonalizing the Hamiltonian;

$E^2(\mathbf{k}) = t^2\, f^{*}(\mathbf{k})f(\mathbf{k}) = t^2\left(1 + e^{-i\mathbf{k}\cdot\mathbf{a_1}} + e^{-i\mathbf{k}\cdot\mathbf{a_2}}\right)\left(1 + e^{i\mathbf{k}\cdot\mathbf{a_1}} + e^{i\mathbf{k}\cdot\mathbf{a_2}}\right)$

$E(\mathbf{k}) = \pm t\sqrt{3 + 2\cos(\mathbf{k}\cdot\mathbf{a_1}) + 2\cos(\mathbf{k}\cdot\mathbf{a_2}) + 2\cos(\mathbf{k}\cdot(\mathbf{a_2} - \mathbf{a_1}))}$, expressing in (x, y) components of k,

$E(k_x, k_y) = \pm t\sqrt{1 + 4\cos\left(\frac{\sqrt{3}ak_y}{2}\right)\cos\left(\frac{ak_x}{2}\right) + 4\cos^2\left(\frac{ak_x}{2}\right)}$, where with lattice constant $a = \sqrt{3}a_0$.

This well-known dispersion relation is illustrated graphically in Figure 2a. At Brillouin zone boundaries, the function f(k) goes to zero.[15] At K points, the solutions of the dispersion relation are degenerate giving zero bandgap between the valence band, and conduction band. Near K points, the transfer Hamiltonian is like the Dirac Hamiltonian, and the dispersion relation is approximately linear, which describes massless quasiparticles.[2]

2.2 Electronic band structure of bilayer graphene in the tight binding approximation

For AB stacked or Bernal bilayer graphene, there are interlayer $2p_z$ orbital interactions between the atoms of the unit cell of the upper layer (1) and lower layer (2). In Figure 1b we illustrate the lattice structure of bilayer graphene along with the relative positions of atoms projected onto the x-y plane. In this bilayer structure, there are now clearly four distinct atoms (A1, B1, A2, and B2). Their electronic coupling can be approximated by considering the intralayer contributions (A1/B1, B1/B2), and the new nearest-neighbor interlayer contributions corresponding to A1/A2 and B1/B2 shown in Figure 1b.[16] Taking four distinct atoms into account (A1, B1, A2, B2) in the tight binding model, Castro et al. and Neto et al. show that the Hamiltonian can be re-expressed as:

$\hat{H} = (-t)\sum_{<i,j>}[a_i^\dagger b_i + a_j^\dagger b_j + HC] - \gamma\sum_{<i,l>}[a_l^\dagger a_i + HC] + \varepsilon\sum_{<i,j>}[a_j^\dagger a_j + b_j^\dagger b_j]$[18, 19]

Here, ε represents the onsite energies, $-t = \langle\varphi_{A1}|\hat{H}|\varphi_{B\,1}\rangle$ is the intralayer transfer integral for electronic hopping between A1 to B1, and A2 to B2 and $-\gamma$ represents the hopping between A1 to A2 ($\langle\varphi_{A1}|\hat{H}|\varphi_{A\,2}\rangle$), and B1 to B2 ($\langle\varphi_{B1}|\hat{H}|\varphi_{B\,2}\rangle$).

Using the Fourier transformed operators; $a_i^\dagger(\vec{r}) = \frac{1}{\sqrt{N}}\sum_{\vec{k}} e^{-i\vec{k}\cdot\vec{r}_{Ai}} a_{\vec{k}}^\dagger$, $b_i^\dagger(\vec{r}) = \frac{1}{\sqrt{N}}\sum_{\vec{k}} e^{-i\vec{k}\cdot\vec{r}_{Bi}} b_{\vec{k}}^\dagger$, and defining vectors $\vec{r}_{Ai} = \vec{R}_i^{A1}$, $\vec{r}_{Bi} = \vec{R}_i^{A1} + \vec{r}_j, \vec{r}_{Al} = \vec{R}_i^{A1} + \vec{r}_4$ it has been shown the approximate Hamiltonian for bilayer graphene is,

$\hat{H} = (-t)\sum_{\vec{r}_j}[e^{i\vec{k}\cdot\vec{r}_j}a_{1\vec{k}}^\dagger b_{1\vec{k}} + e^{i\vec{k}\cdot\vec{r}_j}a_{2\vec{k}}^\dagger b_{2\vec{k}} + e^{-i\vec{k}\cdot\vec{r}_j}b_{1\vec{k}}^\dagger a_{1\vec{k}} + e^{-i\vec{k}\cdot\vec{r}_j}b_{2\vec{k}}^\dagger a_{2\vec{k}}] - \gamma[e^{-i\vec{k}\cdot\vec{r}_4}a_{2\vec{k}}^\dagger a_{1\vec{k}} + e^{i\vec{k}\cdot\vec{r}_4}a_{1\vec{k}}^\dagger a_{2\vec{k}}] + \varepsilon[a_{1\vec{k}}^\dagger a_{1\vec{k}} + a_{2\vec{k}}^\dagger a_{2\vec{k}} + b_{1\vec{k}}^\dagger b_{1\vec{k}} + b_{2\vec{k}}^\dagger b_{2\vec{k}}]$; which can alternately be expressed in matrix form as,

$$\hat{H} = \sum_{\vec{k}}\left(a_{1\vec{k}}^\dagger\ b_{1\vec{k}}^\dagger\ a_{2\vec{k}}^\dagger\ b_{2\vec{k}}^\dagger\right)\begin{pmatrix}\varepsilon_{A1} & -tf(\mathbf{k}) & -\gamma & 0\\ -tf^*(\mathbf{k}) & \varepsilon_{B1} & 0 & 0\\ -\gamma^* & 0 & \varepsilon_{A2} & -tf(\mathbf{k})\\ 0 & 0 & -tf^*(\mathbf{k}) & \varepsilon_{B2}\end{pmatrix}\begin{pmatrix}a_{1\vec{k}}\\ b_{1\vec{k}}\\ a_{2\vec{k}}\\ b_{2\vec{k}}\end{pmatrix} \quad (2)$$

Where, $f(\mathbf{k}) = e^{i\mathbf{k}\cdot\mathbf{r}_1} + e^{i\mathbf{k}\cdot\mathbf{r}_2} + e^{i\mathbf{k}\cdot\mathbf{r}_3}$, and $\varepsilon_{A1}, \varepsilon_{B1}, \varepsilon_{A2}$, and ε_{B2} are onsite energies on atomic sites A1, B1, A2, and B2 respectively. The nearest neighbor vectors are: $\mathbf{r}_1 = a_0\left(\frac{1}{2\sqrt{3}}, \frac{1}{2}, 0\right)$, $\mathbf{r}_2 = a_0\left(\frac{1}{2\sqrt{3}}, -\frac{1}{2}, 0\right)$, $\mathbf{r}_3 = a_0\left(-\frac{1}{\sqrt{3}}, 0, 0\right)$, $\mathbf{r}_4 = b_0(0,0,1)$; giving $f(\mathbf{k}) = e^{\frac{ik_x a_0}{2\sqrt{3}}}(e^{\frac{ik_y a_0}{2}} + e^{-\frac{ik_y a_0}{2}}) + e^{-\frac{ik_x a_0}{\sqrt{3}}} = e^{\frac{ik_x a_0}{2\sqrt{3}}}2\cos(\frac{k_y a_0}{2}) + e^{-\frac{ik_x a_0}{\sqrt{3}}}$.

The 2 X 2 blocks in the upper-left side and the lower-right side of the Hamiltonian in equation (2) represents the intralayer coupling, which looks similar to the monolayer Hamiltonian terms. The 2 X 2 blocks in the upper-right side, and the lower-left side of the Hamiltonian represents interlayer coupling, where the parameter γ describes the coupling between orbitals A1, A2, and/or B1, B2[18]. The parameters $\gamma = 0.14$ eV, $t = 3.16$ eV, and $\varepsilon_{A1}, \varepsilon_{B1}, \varepsilon_{A2}, \varepsilon_{B2} = 0$ in equation (2) have been obtained using infrared spectroscopy[20]. The well-known free electron band structure of AB stacked bilayer graphene is roughly illustrated in the Figure 2b.

Without bias V, $2p_z$ orbital interactions between four atomic sites are responsible for four bands in the dispersion relation as shown in Figure 2c, two for the conduction band, and two for the valence band. The valence band pairs and conduction band pairs are split by the amount of about 0.4 eV, which is an interlayer coupling energy. The splitting occurs due to the strong bonding, and anti-bonding between atomic orbitals A1, A2, and/or B1, B2. The hopping between A1, A2, and/or B1, B2 is responsible for low energy bands. The tight binding model is in good agreement with DFT calculations in the low energy limit[21, 22, 23]. Wang et al. showed that with a potential bias V between two layers of graphene, it is further possible to see the shift in electrochemical potential between the layers[32].

2.3 Effective free electron model: Electronic band structure of *t*BLG

Lastly, we complete our review of the free electron graphene models by considering of the structure of twisted bilayer graphene defined by two layers of AA stacked bilayer graphene rotated around a common site by an arbitrary angle θ. The two lattice vectors for AA stacked bilayer graphene with $\theta = 0°$ are just $\mathbf{a}_1 = a_0\,(1,0)$ and $\mathbf{a}_2 = a_0\left(\frac{1}{2},\frac{\sqrt{3}}{2}\right)$. For non-zero angles the lattice vectors are more complicated because they must span the new superlattice, and are given stacking angle indexed vectors; $\mathbf{a}_1^1 = \mathbf{R}\left(-\frac{\theta}{2}\right)$, and $\mathbf{a}_1^2 = \mathbf{R}\left(\frac{\theta}{2}\right)$.[25] Rotation angle $\theta = 0°$ produces AA stacked bilayer graphene and $\theta = 60°$ corresponds to AB bilayer graphene stacking.

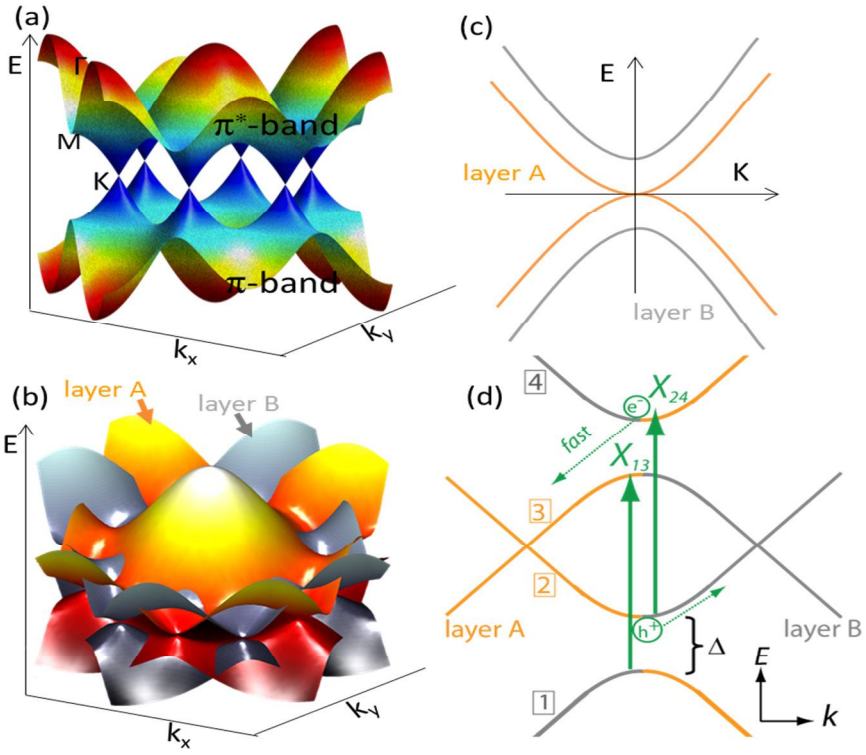

Figure 2. (a) Representation of the band structure for single layer graphene. (b) *t*BLG free electron band-structure, (c) the band dispersion near the K-point in bilayer graphene, (d) cross-sectional view of *t*BLG shows vHS transitions X_{13}, X_{24} between avoided crossing regions.

Rotation angle θ and $-\theta$ produce a similar band structure. *t*BLG does not have a periodic structure in general because of mismatch between the uniformity of layers with respect to each other. The structure is periodic only for some special angles with a well-defined unit cell. A periodic lattice structure of *t*BLG for rotation angles $\theta = 21.8°$, and $\theta = 9.4°$, $\theta = 3.9°$ is shown in Figure 1d, e and f. When the rotation angle is small, the interference between two lattice vectors in two layers gives rise to the pattern called the 'Moiré pattern'[25, 26]. The unit cell is relatively big for small rotation angles as seen in Figures 1e and f. The lattice vectors for a given angle are: $\mathbf{L}_1 = m\mathbf{a}_1^1 + n\mathbf{a}_2^1$; (for layer 1), ; (for layer 2) $\mathbf{L}_2 = R\left(\frac{\pi}{3}\right)\mathbf{L}_1$ and the lattice constant is $L = |L_1| = |L_2| = \frac{|m-n|a}{2\sin(\frac{\theta}{2})}$; where m, n are integers.[24]

For electronic states near the Fermi level, only p_z orbitals needs to be taken into account in the tight binding model. For twisted bilayer graphene, neighbors are rotated with respect to each other (unlike Bernal AB stacking). Therefore, we now have to consider both the ppπ and the ppσ terms to account for the new interlayer interactions between atomic orbitals. As shown by Shallcross et al.[24,25], the Hamiltonian can be written as,

$$\hat{H} = (-1)\sum_{<i,j>} t(R_i - R_j)|R_i><R_j| + HC \qquad (3)$$

where, $t(R_i - R_j)$ is the transfer integral. The transfer integral matrix equations for each type of interlayer orbital interactions are given by: $V_{pp\pi} = -\gamma_0 e^{q_\pi\left(1-\frac{d}{a_0}\right)}$, and $V_{pp\sigma} = \gamma_1 e^{q_\sigma\left(1-\frac{d}{a_1}\right)}$ [26], with the ratio $\frac{q_\sigma}{a_1} = \frac{q_\pi}{a_0}$. Where, a_0 is the nearest neighbor distance, a_1 is the interlayer distance, d is the distance between two orbitals, γ_0 is the transfer integral between nearest neighbors, and γ_1 is the transfer integral between nearest neighbor atoms that are located vertically. Combining these terms, the combined transfer integral is

$-t(R_i - R_j) = V_{pp\pi}\left[1 - \left[\frac{(R_i - R_j)\cdot z}{d}\right]^2\right] + V_{pp\sigma}\left[\frac{(R_i - R_j)\cdot z}{d}\right]^2$ with, $a_0 \approx 0.14$ nm, $a_1 \approx 3.35$ Å, $d \approx 0.335$ nm, $\gamma_0 \approx 2.7$ eV, $\gamma_1 \approx 0.48$ eV, as obtained from literature[26]. Using the above transfer integral, the dispersion relation can be obtained from the determinant of the Hamiltonian of equation (3).[13] A rough illustration of the resulting free electron interlayer band structure of *t*BLG is shown in Figure 2b. There is an anti-crossing where bands of two layers meet. This anti-crossing is a result of interlayer interactions between the layers.

Figure 2d sketches the cross-section view of the band structure, showing the van Hove Singularity (vHS) transitions X_{13} and X_{24}. The bands near K, and K′ come from single layer graphene (layer 1, and layer 2), and they are folded into the same Brillouin zone. These bands don't mix with each other giving rise to the linear dispersion relation near K, and K′. Near the M point, there is a splitting in energy due to anti-crossing of the bands. The allowed optical transitions are also shown. The band structure of *t*BLG for different rotation angles look similar, however, the overall energy decreases by minimizing the rotation angle. The splitting energy near the M-point is of the order of interlayer coupling between the two layers, which is about 0.2 eV for all possible rotation angles.[15] For rotation angles $< 1°$, parabolic dispersion is obtained. For rotation angles around 1°, there bands are flat near the Fermi level. There is a transition from parabolic to linear dispersion for rotation angles $1° \leq \theta \leq 2°$. For angles above 10° and up to the symmetric point of 30°, the dispersion is linear as in single layer graphene at the K point[27].

2.4 Review of bound exciton model for *t*BLG

Upon photoexcitation of *t*BLG, exciton effects may manifest themselves owing to Coulombic interactions of e-h pairs. To theoretically model the many-body excitonic effects, it is necessary to solve the BSE as shown by Rohlfing et al.[28]: $(E_{ck} - E_{vk})A^S_{vck} + \sum_{v'c'k'}\langle vck|K^{eh}|v'c'k'\rangle A^S_{v'c'k'} = \Omega^S A^S_{vck}$, where, A^S_{vck} is the exciton wave function in k-space, Ω^S is the exciton eigenenergy, K^{eh} is the e-h interaction kernel, and $|vk\rangle, |ck\rangle$ are the hole and electron states, respectively. In order to predict possible bound exciton states, it is important to know the e-h attractive energy E^S_a, which roughly corresponds to the binding energy, and recently the first-principle BSE simulations in Liang et al.[14] reported that $E^S_a = 0.5\ eV$ for 21.8° *t*BLG.

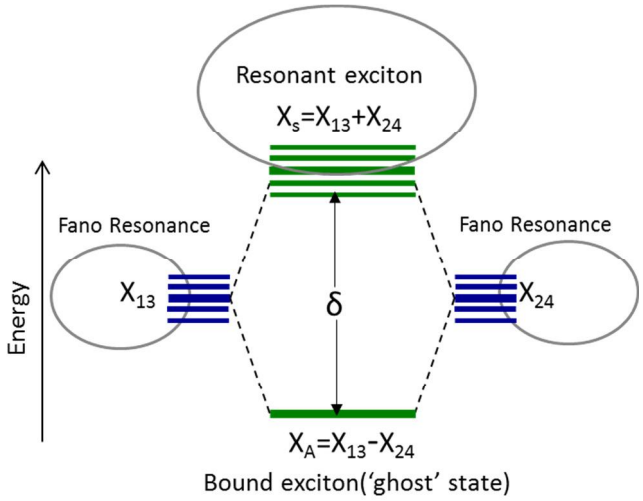

Figure 3. Upon resonant optical excitation, degenerate Fano resonance states X_{13} and X_{24} rehybridize producing a higher energy resonant exciton state X_s and lower energy bound exciton state X_A.

Specifically, Liang et al. solved for $E_a^S = \langle S|K^{eh}|S\rangle = \sum_{vck}(E_{ck} - E_{vk})|A_{vck}^S||A_{vck}^S| - \Omega^S$, which is the net exciton kinetic energy plus the weighted single-particle band energy difference between electrons and holes[14]. To simplify the direct analysis of the first principle BSE simulation, low-energy effective model is often further assumed, giving a simpler perturbed Hamiltonian that is analogous to Equation (1), specfically[29];

$$H(k) = \begin{pmatrix} H_0(k,0) & T^+ \\ T & H_0(k-\Delta K,\theta) \end{pmatrix}, \text{ with } H_0(k,0) = \hbar v_F \begin{pmatrix} 0 & e^{-i\theta}(k_x - ik_y) \\ e^{i\theta}(k_x + ik_y) & 0 \end{pmatrix}, \text{ where } T = \Delta \begin{pmatrix} 0 & 1 \\ 1 & 0 \end{pmatrix} \quad (4)$$

The average interlayer interaction between AB and BA stacking order is described by matrix T with interlayer coupling strength Δ. The low-energy effective model is best for small-twisting angles because the linear Dirac-Fermion dispersion is preserved. Using the BSE and the low effective model, Liang et al.[14] found that upon resonant excitation of *t*BLG, you can access degenerate Fano resonant transitions X_{13}, X_{24} shown in Figure 2d which then effectively rehybridize as depicted in Figure 3. The symmetric superposition of the two degenerate transitions give rise to a higher energy bright state and anti-symmetric superposition give rise to the lower energy dark state ('ghost' state, see figure 3). The constructive interference couples with the lower lying continuum which broadens the resulting resonant bright excitonic state. The antisymmetric superposition cancels the coupling between the lower lying continuum making it a localized bound excitonic state. The so-called ghost Fano resonance effect was found in quantum dot molecules.[30] This model is appropriate for small twist angle, however, the double resonance of transitions and the destructive interference plays crucial role in existence of strongly bound excitons.[14] The formation mechanism of this dark state X_A is very general, and may hold exciting promise for other twisted stacked 2D vdW materials.

3. EXPERIMENTAL

To experimentally test which model (sections 2.3 vs. 2.4) best describes the resonant excited state of *t*BLG best we perform ultrafast microscopy measurements on single-grain of tBLG. We begin with multilayer graphene grown using CVD method on copper foil and then transferred to silicon nitride grids, silicon or fused silica. Transient absorption (TA) microscopy on *t*BLG requires (*i*) identification of large-area *t*BLG regions (*ii*) probe-beam diffraction limited resolution TA. Single-grain regions of *t*BLG were identified using diffraction-limited scanning confocal TA microscopy with 120 fs delayed pulses. *t*BLG regions were detected by exciting above resonance and probing well-below resonance (typically at 0.8 eV). *t*BLG regions show a markedly enhanced TA when the resonance lies between the pump and probe beam energies, owing to the strong electronic relaxation bottleneck effect in the interlayer *t*BLG states.

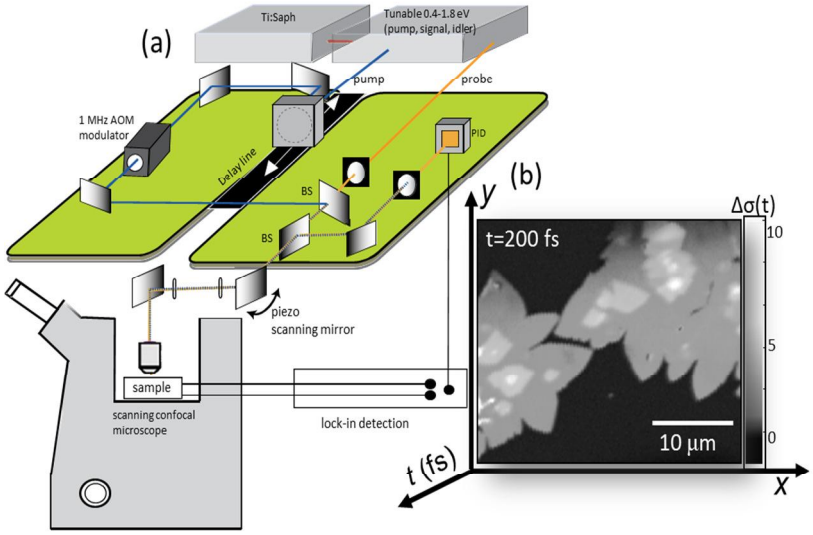

Figure 4. (a) Optical setup for transient absorption (TA) microscopy. Sub-diffaction limited pump, and probe pulses are raster scanned , and the sample can be imaged against the laser noise floor by employing a lock-in amplifer detection synched to an acousto-optical (AO) modulator (1 MHz), (b) Stacked TA images for a movie of the localized electronic decay.

After the regions with anomalous electronic relaxation dynamics are identified, the precise absorption resonances were later measured using hyperspectral absorption imaging.[31] By collecting the full-frame absorption movies, specific absorption spectra can be acquired by integrating over a defined region, and plotting as a function of absorbing wavelength. The correspondence between absorption resonance and twist angle has been previously established[12,31]. Once all optical measurements were complete, darkfield transmission electron microscopy (TEM) was used to determine precise angle assignments and a composite image is constructed. Similar results were obtained for *t*BLG on silicon, silicon nitride and fused silica substrates.

Scanning confocal ultrafast transient absorption (TA) microscopy enables us to simultaneously obtain near diffraction-limited spatial resolution while also have sub-time resolution. This enabled us to study the electron relaxation dynamics in single-grain of graphene. In Figure 3a and 3b, we show bilayer CVD graphene locally excited with a modulated (1 MHz) 140 fs pump pulse at 980 nm. We then probe graphene at 1650 nm using a second collinear probe pulse at some time-delay, *t*. By collecting the change in reflectance ($\Delta R(t)$) of the probe pulse we plot the dynamics of graphene in both space and time. By stacking the frames in Figure 3b, we can reconstruct a 'movie' of photoexcited hot electrons relaxing. This electron-relaxation 'movie' is also a novel fast imaging technique for nanomaterials, and requires only seconds to acquire each frame.

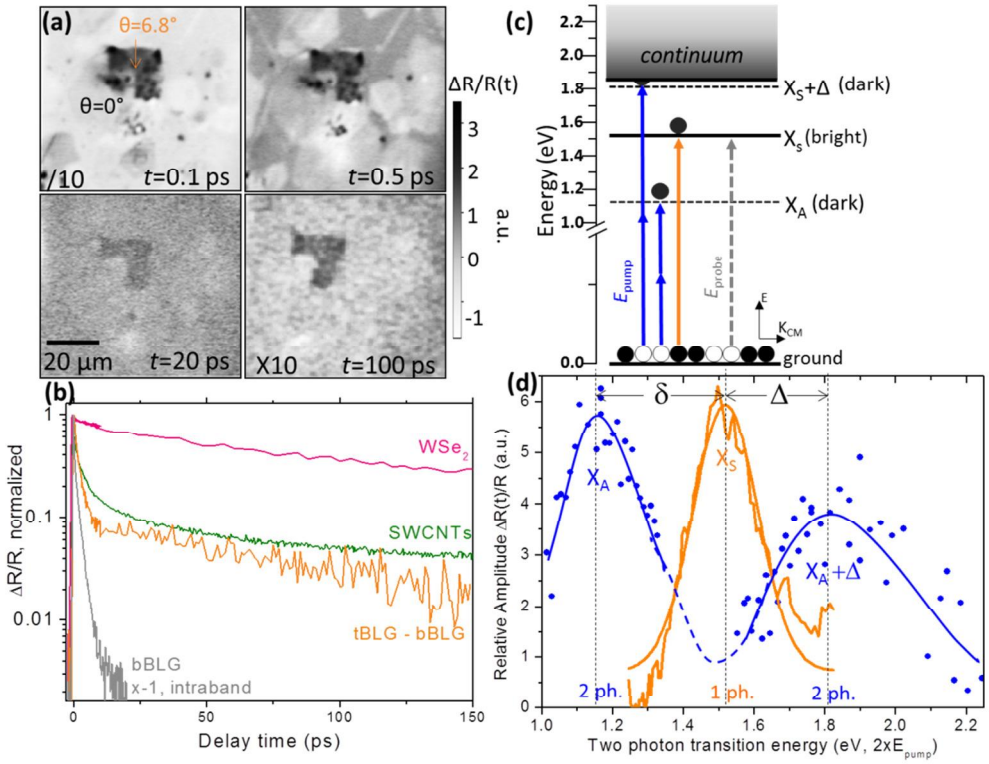

Figure 5 a. Transient Absorption (TA) microscopy maps at each time-delay show a greatly enhanced, long-lived electronic population localized to the 6.8° *t*BLG grain shown. Video 1 shows resonantly pumped and probed *t*BLG showing strong evidence of an electron relaxation bottleneck in the vicinity of the expected avoided crossing van Hove singularity optical resonances (http://dx.doi.org/10.1117/12.2262003). b. Comparative TA relaxation kinetics of resonantly excited tBLG (orange), bBLG (gray), (6,5) SWCNTs, and few layer WSe2. c. Bound exciton model d. Two-photon TA spectrum of 8°tBLG, showing higher lying state at 1.82 eV and lower lying state at 1.12 eV (blue). One-photon absorption spectrum (orange) subtracted from the absorptive contribution of Bernal bilayer graphene.

4. RESULTS AND DISCUSSION

When two sheets of graphene stack, the interlayer electronic states hybridize, resulting in a prominent visible absorption peak that is tunable with the stacking angle. Recent first principle Bethe-Salpeter simulations of twisted bilayer graphene, predict that interlayer electronic orbitals interfere destructively to form stable, strongly bound exciton states[32]. While this excitonic model corroborates the experimental absorption line shape observed[33], the actual existence of strongly- bound excitons in an otherwise metallic system remains controversial and untested.

To test these conflicting models[34], we use one and two-photon confocal scanning transient absorption (TA) microscopy as an incisive space-time probe of both the *t*BLG interlayer state energies and electronic population. Figure 5 unambiguously demonstrates the existence of manifold of bright and dark interlayer states that create a critical energy relaxation bottleneck in resonantly excited *t*BLG. As shown in Figure 5a, upon resonant excitation at t=0.1 ps, we observe a strong positive signed interband transient response from *t*BLG grain. By contrast, the surrounding Bernal stacked bilayer graphene (*b*BLG) gives a comparatively weak the weak negative signed intraband contribution to the transient optical conductivity. The roughly bi-exponential decay may be comparable to known excitonic systems like single-walled carbon nanotube (SWCNT). However as shown in Figure 5d, *t*BLG relaxation kinetics are highly dissimilar from *b*BLG and show a distinct relaxation bottleneck. One and two-photon TA spectrum of *t*BLG 8° domain is shown in Figure 5d showing one state above and one below (blue) the bright state resonance (orange). These results support recent theory[13] outlined in section 2.4 that advocate for strongly bound, stable excitons in *t*BLG. Specifically, it shows a strongly-bound exciton model works best as evidenced by; *i*. the radically enhanced and long-lived electronic population in Figure 5a, b, *ii*. bright/dark state asymmetry[34] in Figure 5d, and *iii*. rigorously enforced one- and two-photon selection rules in Figures 5c-d. Collectively, this suggests that not unlike SWCNTs, *t*BLG electronic structure may also be dominated by a low-lying, strongly-bound exciton state[13,34,35].

5. CONCLUSIONS

We have demonstrated how you can access different interlayer functionalities of vdW materials by stacking and twisting two monolayers. Upon stacking two graphene sheets together in a minimum energy configuration, it is well known that you obtain massive chiral quasiparticles with parabolic dispersion relation for low energy, and the bands touch at zero energy. Our work concerns when you have two sheets of graphene stacked at angle θ. In this twisted configuration, the velocity of photoexcited electrons can change as a function of the rotation angle owing to an avoided crossing region that creates interlayer electronic states. For the free-electron band structure model, these avoided crossing regions give vHs-like resonances that have been known since 2009[32] to resonantly enhance the optical ~20% oscillator strength. In this work, we consider how many body interactions become important in *t*BLG by presenting further evidence that is able to form bound excitons.

Our ultrafast microscopy results lends experimental support to a theoretical model put forward by Liang et al.[14] that predicts that bound excitons occur from a cancellation of exciton-continuum coupling (often referred to as a 'ghost' Fano resonance effect). Our transient absorption microscopy was able to 'film' the journey of electrons once photoexcited at the *t*BLG resonances. The high population and long carrier relaxation in *t*BLG is strikingly different than AB stacked BLG, suggesting some of the resonantly excited carriers are not coupled to the lower lying continuum sates. We referred to this observation as an electron relaxation bottleneck that can be best explained by the existence of a lower lying state located at 0.37 eV below the bright state resonance for 8.7° *t*BLG domain. In our model, the photoexcited carriers can populate a symmetrically hybridized interlayer exciton state by 1-photon resonant excitation. Subsequently, these excitons relax impulsively to the bound antisymmetric strongly-bound exciton state that is optically dark to 1-photon excitation. Our results support that such states are weakly coupled to the continuum, forming a quasi-stable exciton with an appreciable lifetime. These new experimental observations provide new evidence to support recently works[33,34] that suggests *t*BLG is a novel van der Waals material where free electrons can co-exist with bound excitons upon resonant excitation. The growing evidence for this double resonance picture creating bound interlayer excitons is very general and may hold exciting promise for other stacked, twisted 2D vdW materials. Control over the stacking and twisting of 2D vdW materials offers a new degree of freedom that is inaccessible with traditional 3D bulk materials. For *t*BLG, the collective preliminary research suggests exciting applications for fast photosensitive devices requiring both stable excitons and hybrid metallic properties.

ACKNOWLEDGMENTS

This research work was supported in part by a grant from the Spectroscopy Society of Pittsburgh, Oregon BEST and ONAMI. Material fabrication was supported by Cornell's AFOSR (FA 9550-10-1-0410) grant. We thank Li Yang at University of Washington, St. Louis for helpful discussions.

REFERENCES

[1] K. S. Novoselov, A. K. Geim, S. V. Morozov, D. Jiang, Y. Zhang, S. V. Dubonos, I. V. Grigorieva, and A. A. Firsov, "Electric field effect in atomically thin carbon films," Science 306(5696), pp. 666–669, 2004.

[2] K. Novoselov, D. Jiang, F. Schedin, T. Booth, V. Khotkevich, S. Morozov, and A. Geim, "Two-dimensional atomic crystals," Proceedings of the National Academy of Sciences of the United States of America 102(30), pp. 10451–10453, 2005.

[3] C. Lee, X. Wei, J. W. Kysar, and J. Hone, "Measurement of the elastic properties and intrinsic strength of monolayer graphene," Science 321(5887), pp. 385–388, 2008.

[4] I. Meric, M. Y. Han, A. F. Young, B. Ozyilmaz, P. Kim, and K. L. Shepard, "Current saturation in zerobandgap, top-gated graphene field-effect transistors," Nature Nanotechnology 3(11), pp. 654–659, 2008.

[5] D. DiVincenzo and E. Mele, "Self-consistent effective-mass theory for intralayer screening in graphite intercalation compounds," Physical Review B 29(4), p. 1685, 1984.

[6] G. W. Semenoff, "Condensed-matter simulation of a three-dimensional anomaly," Physical Review Letters 53(26), p. 2449, 1984.

[7] M. Katsnelson, "Zitterbewegung, chirality, and minimal conductivity in graphene," The European Physical Journal B-Condensed Matter and Complex Systems 51(2), pp. 157–160, 2006.

[8] K. S. Novoselov, E. McCann, S. Morozov, V. I. Falko, M. Katsnelson, U. Zeitler, D. Jiang, F. Schedin, and A. Geim, "Unconventional quantum hall effect and berrys phase of 2π in bilayer graphene," Nature Physics 2(3), pp. 177–180, 2006.

[9] T. Ohta, A. Bostwick, T. Seyller, K. Horn, and E. Rotenberg, "Controlling the electronic structure of bilayer graphene," Science 313(5789), pp. 951–954, 2006.

[10] L. Brown, R. Hovden, P. Huang, M. Wojcik, D. A. Muller, and J. Park, "Twinning and twisting of tri-and bilayer graphene," Nano Letters 12(3), pp. 1609–1615, 2012.

[11] A. Reina, X. Jia, J. Ho, D. Nezich, H. Son, V. Bulovic, M. S. Dresselhaus, and J. Kong, "Large area, few-layer graphene films on arbitrary substrates by chemical vapor deposition," Nano Letters 9(1), pp. 30–35, 2008.

[12] R. W. Havener, H. Zhuang, L. Brown, R. G. Hennig, and J. Park, "Angle-resolved raman imaging of interlayer rotations and interactions in twisted bilayer graphene," Nano Letters 12(6), pp. 3162–3167, 2012.

[13] M. W. Graham, S.-F. Shi, Z. Wang, D. C. Ralph, J. Park, and P. L. McEuen, "Transient absorption and photocurrent microscopy show that hot electron supercollisions describe the rate-limiting relaxation step in graphene," Nano Letters 13(11), pp. 5497–5502, 2013.

[14] Y. Liang, R. Soklaski, S. Huang, M. W. Graham, R. Havener, J. Park, and L. Yang, "Strongly bound excitons in gapless two-dimensional structures," Physical Review B 90(11), p. 115418, 2014.

[15] S. Reich, J. Maultzsch, C. Thomsen, and P. Ordejón, "Tight-binding description of graphene" Phys. Rev. B 66, 035412, 2002.

[16] K. Takase, S. Tanabe, S. Sasaki, H. Hibino, and K. Muraki, "Transport spectroscopy of epitaxial graphene on sic using quantum capacitances," in Proceedings of the 12th Asia Pacific Physics Conference (APPC12), p. 012065, 2014.

[17] P. R. Wallace, "The band theory of graphite," Physical Review 71(9), p. 622, 1947.

[18] E. V. Castro, K. Novoselov, S. Morozov, N. Peres, J. L. dos Santos, J. Nilsson, F. Guinea, A. Geim, and A. C. Neto, "Electronic properties of a biased graphene bilayer," Journal of Physics: Condensed Matter 22(17), p. 175503, 2010.

[19] A. C. Neto, F. Guinea, N. M. Peres, K. S. Novoselov, and A. K. Geim, "The electronic properties of graphene," Reviews of Modern Physics 81(1), p. 109, 2009.

[20] A. Kuzmenko, I. Crassee, D. Van Der Marel, P. Blake, and K. Novoselov, "Determination of the gate-tunable band gap and tight-binding parameters in bilayer graphene using infrared spectroscopy," Physical Review B 80(16), p.

165406, 2009.
[21] H. Min, B. Sahu, S. K. Banerjee, and A. MacDonald, "Ab initio theory of gate induced gaps in graphene bilayers," Physical Review B 75(15), p. 155115, 2007.
[22] S. Latil and L. Henrard, "Charge carriers in few-layer graphene films," Physical Review Letters 97(3), p. 036803, 2006.
[23] M. Aoki and H. Amawashi, "Dependence of band structures on stacking and field in layered graphene," Solid State Communications 142(3), pp. 123–127, 2007.
[24] P. Moon and M. Koshino, "Optical absorption in twisted bilayer graphene," Physical Review B 87(20), p. 205404, 2013.
[25] S. Shallcross, S. Sharma, E. Kandelaki, and O. Pankratov, "Electronic structure of turbostratic graphene," Physical Review B 81(16), p. 165105, 2010.
[26] T. Green and J. Weigle, "Theorie du moire," in Helvetica Physica Acta, 21(3-4), pp. 217–217, 1948.
[27] G. Trambly de Laissardiere, D. Mayou, and L. Magaud, "Localization of dirac electrons in rotated graphene bilayers," Nano Letters 10(3), pp. 804–808, 2010.
[28] M. Rohlfing and S. G. Louie, "Electron-hole excitations and optical spectra from first principles," Physical Review B 62(8), p. 4927, 2000.
[29] E. J. Mele, "Band symmetries and singularities in twisted multilayer graphene," Physical Review B 84(23), p. 235439, 2011.
[30] M. L. De Guevara, F. Claro, and P. A. Orellana, "Ghost fano resonance in a double quantum dot molecule attached to leads," Physical Review B 67(19), p. 195335, 2003.
[31] R. W. Havener, C.-J. Kim, L. Brown, J. W. Kevek, J. D. Sleppy, P. L. McEuen, and J. Park, "Hyperspectral imaging of structure and composition in atomically thin heterostructures," Nano Letters 13(8), pp. 3942– 3946, 2013.
[32] Y. Zhang, T.-T. Tang, C. Girit, Z. Hao, M. C. Martin, A. Zettl, M. F. Crommie, Y. R. Shen, and F. Wang, "Direct observation of a widely tunable bandgap in bilayer graphene," Nature 459(7248), pp. 820–823, 2009.
[33] R. W. Havener, Y. Liang, L. Brown, L. Yang, and J. Park, "Van hove singularities and excitonic effects in the optical conductivity of twisted bilayer graphene," Nano Letters 14(6), pp. 3353–3357, 2014.
[34] H. Patel, R. W. Havener, L. Brown, Y. Liang, L. Yang, J. Park, and M. W. Graham, "Tunable optical Excitations in twisted bilayer graphene form strongly bound excitons," Nano Letters 15(9), pp. 5932-5937, 2015.
[35] K. Vogt, S. Shi, F. Wang, M. W. Graham, "Dynamic Resolution of Photocurrent Generating Pathways by Field-Dependent Ultrafast Microscopy," OSA Technical Digest, Ultrafast Phenomena, DOI:10.1364/UP.2016.UW2A.3, 2016.